Int J Adv Manuf Technol (2007) 34:483–490
DOI 10.1007/s00170-006-0625-0

ORIGINAL ARTICLE

Aspheric surface finishing by fixed abrasives

Hon-Yuen Tam · Meng Hua · Lei Zhang

Received: 11 June 2005 / Accepted: 18 March 2006 / Published online: 25 August 2006

Abstract This paper presents a method for the finishing of aspheric surfaces using fixed abrasives. The strategy is to remove a specified amount of material from the surface. The method assumes concentric tool paths perpendicular to the axis of the surface. The key parts of the method are: (1) efficient computation of the material removal profile for each tool path and (2) optimisation of the feed rate for the tool paths. Simulation results are included to illustrate the proposed method, which suggest that the method is potentially useful for aspheric surface finishing.

Keywords Aspheric surface finishing · Fixed abrasives · Hertzian contact

1. Introduction

Surface finishing is required for the manufacturing of many metallic products. Subsequent to the forming of the parts, they need to be surface finished for the removal of machine marks and burrs, as well as for the improvement of the surface finishing.

H.-Y. Tam (✉) · M. Hua
Department of Manufacturing Engineering and Engineering Management, City University of Hong Kong,
83 Tat Chee Avenue,
Kowloon Tong, Hong Kong, People's Republic of China
e-mail: hon.y.tam@cityu.edu.hk

L. Zhang
School of Mechanical Science and Engineering,
Nanling Campus, Jilin University,
Changchun 130025 Julin, People's Republic of China

Fixed abrasives, filamentary brushes and loose abrasives are common approaches to surface finishing [1–6]. Surface finishing automation can be realised by numerical control of the tool across the surface based on pre-planned tool paths [7–9].

For surface finishing using fixed abrasives, the material removal approximately follows Archard's wear law. That is, the rate of material removal is proportional to the pressure at the contact between the tool and the surface. Moreover, for fixed abrasives working on metallic surfaces, the contact stress was adequately approximated by Hertzian contact for tools of highly elastic binding materials on the part surfaces of steel [10]. The contact is elliptic; when the material of the tool and of the surface are fixed, the size and orientation of the ellipse depends on the force normal to the contact.

The material removal profile at a point of the tool path is the depth of material removed along the direction orthogonal to the tool path. It depends on the tool and local surface geometry, on the tool path, as well as on process parameters, such as spindle speed, feed rate and the normal force. The model in Zhang et al. [10] was adapted to construct the material removal profile by integrating the abrasion of the tool at each location of the surface for a given tool path and set of process parameters [11, 12].

There are many applications for the finishing of aspheric surfaces. Examples are the post-processing of machined parts after turning and the polishing of moulds for optical lenses and of surfaces with one axis of revolution.

This paper follows the work in material removal profile computation [12]. The purpose of this paper is to develop a method for finishing aspheric surfaces by fixed abrasives. The paper starts by summarising the previous work [12]. The main parts of the proposed method are simplifications for the profile computation for aspheric surfaces and the

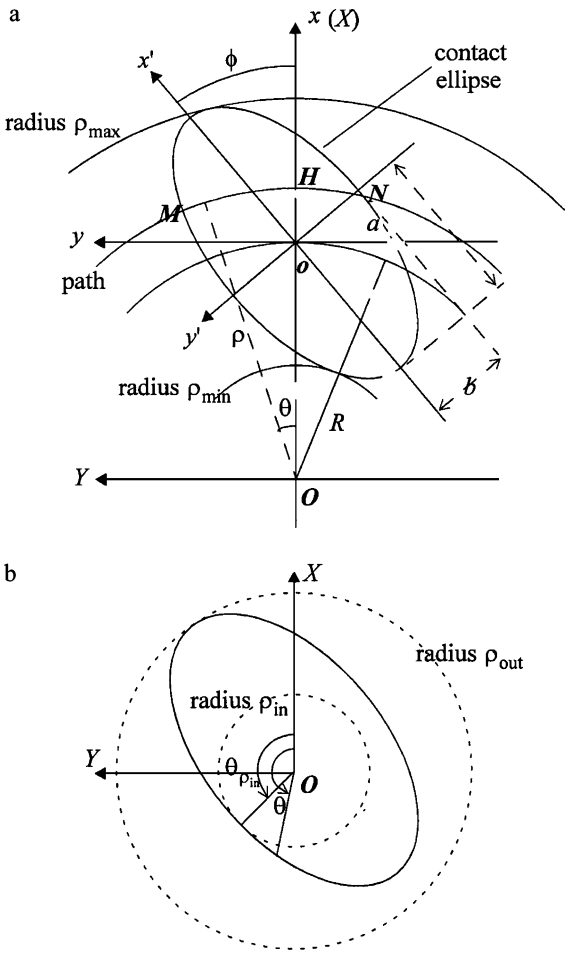

Fig. 1a, b Geometric entities at the contact with the centre of geodesic curvature (**a**) outside and (**b**) inside the contact

generation of tool motion parameters for aspheric surface finishing. Application examples will be presented to illustrate the proposed method.

2. Material removal profile

This section summarises the previous work in removal profile computation [12]. Figure 1a shows the contact between the tool and the part surface. For a path point o on a part surface, frame x–o–y is centred at o and fixed to the part surface such that the y axis is tangential to the tool path and the z axis is normal to the surface at o. Under the assumption of Hertzian contact between the tool and the part surface, the contact is elliptic with the principal axes of the contact ellipse along the x' and y' axes, a and b being the major and minor axes, respectively, and ϕ being the angle between the x and x' axes. These contact parameters depend on the local geometry and material properties of the tool and the surface, as well as on the normal force at the contact. Through transformation from frame x'–o–y' to frame x–o–y and then to frame X–O–Y, the ellipse may be written in polar coordinates (ρ,θ) as:

$$m(\rho\cos\theta - \mathrm{R})^2 + l(\rho\cos\theta - \mathrm{R})\rho\sin\theta + \mathrm{n}\rho^2\sin^2\theta - a^2b^2 = 0 \tag{1}$$

where:

$$\begin{aligned} m &= a^2\sin^2\phi + \mathrm{b}^2\cos^2\phi \\ l &= \left(b^2 - a^2\right)\sin 2\phi, \\ n &= a^2\cos^2\phi + \mathrm{b}^2\sin^2\phi \end{aligned} \tag{2}$$

R is the geodesic radius of curvature. The centre of the geodesic curvature O is obtained by moving point o by a distance R along the negative x direction.

Assuming that the processing parameters (i.e. the normal force, spindle speed), tool motion (i.e. the tool speed and orientation and tool path curvature) and the surface geometry do not change significantly in the vicinity of o such that the relative orientation and size of the contact ellipse do not change significantly in that vicinity, the material removal at point H on the surface along the x axis may be approximated by integrating the material removal along the part(s) of the circle centred at O with radius ρ that falls within the ellipse (i.e. $\overset{\frown}{MN}$ and the circle/ellipse intersections are at $\theta=\theta_1$ and θ_2):

$$h(\rho) = \frac{3k_{abr}F_nVR}{2\pi H_v V_{f0}(ab)^2}\int_{\theta_1(\rho)}^{\theta_2(\rho)} f(\theta)d\theta, \tag{3}$$

for $\rho_{min} \le \rho \le \rho_{max}$

where $h(\rho)$ represents the depth of removal for a given ρ:

$$f(\theta) = \sqrt{\begin{array}{c} a^2b^2 - m(\rho\cos\theta - \mathrm{R})^2 \\ -l(\rho\cos\theta - \mathrm{R})\rho\sin\theta - \mathrm{n}\rho^2\sin^2\theta \end{array}} \tag{4}$$

k_{abr} is a dimensionless wear coefficient, F_n is the normal force, H_v is the hardness of the surface, V is the spindle speed of the tool and V_{f0} is the feed rate of the tool along the path.

For the case of O lying within the contact ellipse (Fig. 1b), the material removal profile in Eq. 3 is defined for $\rho \le \rho_{\mathrm{out}}$. For $\rho \le \rho_{\mathrm{in}}$, $f(\theta)$ is to be integrated over the range $[0, 2\pi]$, and for $\rho_{\mathrm{in}} < \rho < \rho_{\mathrm{out}}$, it is to be integrated over the part(s) of the circle centred at O with radius ρ that falls within the ellipse.

For a given path and contact, the removal profile $h(\rho)$ is computed numerically. For instance, a numerical search is employed to establish $\rho_{\min}$ and $\rho_{\max}$ in Fig. 1a. Then, for a given ρ within $(\rho_{\min}, \rho_{\max})$, the bounds $\theta_1(\rho)$ and $\theta_2(\rho)$ of the integral in Eq. 3 are determined numerically. Having determined the bounds, the integral in Eq. 3 can then be solved numerically (i.e. using the five-point Gaussian approximation).

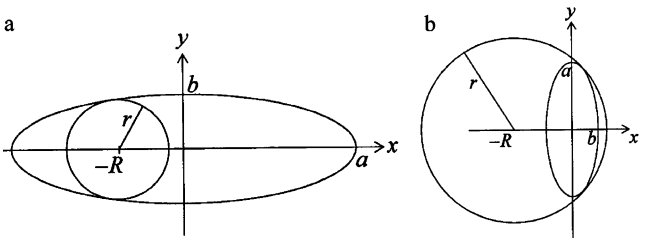

Fig. 2a, b Ellipse and circle contact with the major axis of the ellipse along (**a**) the x and (**b**) the y axes

3. Material removal profile for aspheric surfaces

To determine each point of a material removal profile requires a numerical search for the bounding values $\rho_{\min}$, $\rho_{\max}$, $\theta_1(\rho)$ and $\theta_2(\rho)$ in Eq. 3 and ρ_{in} and ρ_{out} in Fig. 1b. Computing the profile along a tool path could be rather computationally intensive.

For finishing aspheric surfaces, an obvious choice of tool paths are circular rings on the surface that are perpendicular to the axis of the surface, and the tool axis is co-planar with that axis. This results in the major axis of the contact ellipse between the tool and the surface either along the meridians of the surface (ϕ=0°) or along the parallels of the surface (ϕ=90°). This section considers an analytic approach to determine those bounds of the integral.

3.1. Circle and ellipse contacts

The equations for a circle and an ellipse in contact (Fig. 2a) are given by:

$$(x+R)^2 + y^2 = r^2 \tag{5}$$

and:

$$\frac{x^2}{a^2} + \frac{y^2}{b^2} = 1 \tag{6}$$

such that the major axis of the ellipse is along the axis and the centre of the circle is on the negative x -axis. When a, b and R are fixed, the radius r of the circle and the location of contact (x, y) can be deduced from these two equations and a third equation is obtained by requiring dy/dx of both equations to be equal at the contact, i.e.:

$$\frac{-(x+R)}{y} = \frac{-b^2 x}{a^2 y} \Rightarrow x = -\frac{a^2 R}{a^2 - b^2} \tag{7}$$

One then has y from Eqs. 6 and 7 as:

$$y = \pm b\sqrt{1 - \frac{a^2 R^2}{(a^2 - b^2)^2}} \tag{8}$$

and r from Eqs. 5, 7 and 8 as:

$$r = b\sqrt{1 - \frac{R^2}{a^2 - b^2}} \tag{9}$$

Equation 8 is valid only for:

$$1 - \frac{a^2 R^2}{(a^2 - b^2)^2} \geq 0 \Rightarrow R \leq \frac{a^2 - b^2}{a} \tag{10}$$

This also implies that Eq. 9 is restricted to:

$$r \geq \frac{b^2}{a} \tag{11}$$

It is noted that the radius of curvature of the ellipse is smallest at $(-a, 0)$, which is exactly b^2/a. One concludes that, for $0 \leq R < (a^2-b^2)/a$, the circle and the ellipse contact at two locations and Eqs. 7, 8, 9 can be used to calculate (x, y, r). For $R=(a^2-b^2)/a$, the radius r is b^2/a and the circle and the ellipse contact at one location only, i.e. at $(-a, 0)$. For $(a^2-b^2)/a < R < a$, the contact location remains unchanged at $(-a, 0)$ and $r=a-R$.

For the circle and ellipse contact in Fig. 2b such that the major axis of the ellipse is along the y axis, the equation of the circle is the same as in Eq. 5 and the ellipse in Fig. 2b assumes the form:

$$\frac{x^2}{b^2} + \frac{y^2}{a^2} = 1 \tag{12}$$

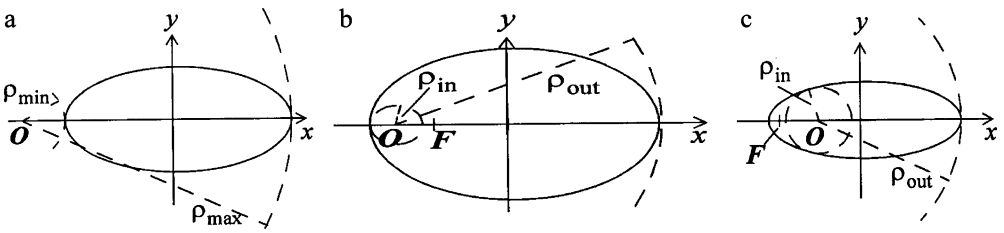

Fig. 3a–c Radii of the material removal profile with ϕ=0°: (**a**) $\rho_{\min}$ and $\rho_{\max}$ for $R>a$. ρ_{in} and ρ_{out} for (**b**) $a>R>(a^2-b^2)/a$ and (**c**) $a>(a^2-b^2)/a>R$

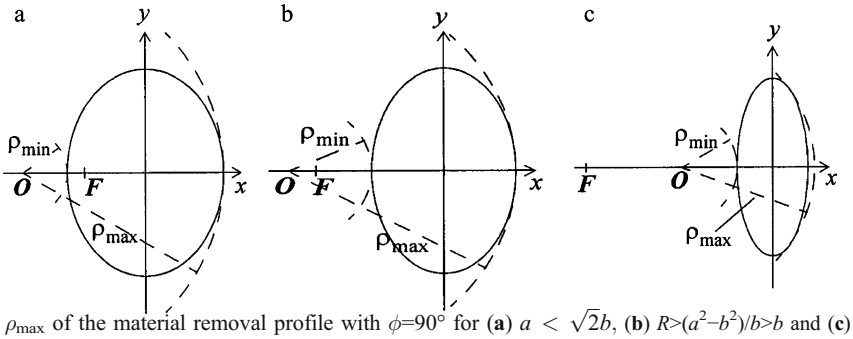

Fig. 4a–c Radii ρ_{min} and ρ_{max} of the material removal profile with ϕ=90° for (**a**) $a < \sqrt{2}b$, (**b**) $R>(a^2-b^2)/b>b$ and (**c**) $(a^2-b^2)/b>R>b$

Through a similar analysis, one obtains:

$$x = -\frac{b^2 R}{a^2 - b^2} \tag{13}$$

$$y = \pm a\sqrt{1 - \frac{b^2 R^2}{(a^2 - b^2)^2}} \tag{14}$$

and:

$$r = a\sqrt{1 + \frac{R^2}{a^2 - b^2}} \tag{15}$$

for the contact locations (x, y) and the radius of circle r. Again, Eq. 14 is valid only for:

$$1 - \frac{b^2 R^2}{(a^2 - b^2)^2} \geq 0 \Rightarrow R \leq \frac{a^2 - b^2}{b} \tag{16}$$

which restricts:

$$r \leq \frac{a^2}{b} \tag{17}$$

by Eq. 15. One observes that the radius of curvature of the ellipse is largest at (b, 0), which is exactly a^2/b. Thus, for $0 \leq R < (a^2-b^2)/b$, the circle and the ellipse contact at two locations and Eqs. 13, 14, 15 can be used to calculate (x, y, r). For $(R=(a^2-b^2)/b$, r is a^2/b; the circle and the ellipse contact at (b, 0). For $R>(a^2-b^2)/b$, the contact location remains unchanged at (b, 0) and $r=R+b$. Also, the centre of the circle is outside (or inside) the ellipse if $R=(a^2-b^2)/b>b$ (or $<b$), which implies $a > \sqrt{2}b$ (or $< \sqrt{2}b$).

3.2. Major axis of the contact ellipse along the meridians

The major axis of the contact ellipse is along the x direction when ϕ=0°. In this case, (m, n, l)=(b^2, a^2, 0) for Eq. 2. Equation 4 becomes:

$$f(\theta) = \sqrt{a^2 b^2 - b^2(\rho\cos\theta - \mathrm{R})^2 - a^2\rho^2\sin\theta^2} \tag{18}$$

Point O lies outside the ellipse when $R>a$, as illustrated in Fig. 3a. The range of ρ in Eq. 3 is within (ρ_{min}, ρ_{max}), where $\rho_{min}=R-a$ and $\rho_{max}=R+a$ are the radii of the circles centred at O and they touch the ellipse at one point only.

Equation 1 can be written as:

$$\begin{aligned}\left(a^2 - b^2\right)\rho^2(\cos\theta)^2 + 2b^2\rho R\cos\theta \\ +\left(a^2b^2 - a^2\rho^2 - b^2R^2\right) = 0\end{aligned} \tag{19}$$

which is quadratic in $\cos\theta$. For $\rho_{min}<\rho<\rho_{min}$, there is only one solution of $\cos\theta$ within (−1, 1) and the integral in Eq. 3 becomes:

$$2\int_0^{\theta_b} f(\theta)\,\mathrm{d}\,\theta \tag{20}$$

where $\theta_b \in (0, \pi)$ corresponds to that solution of Eq. 19.

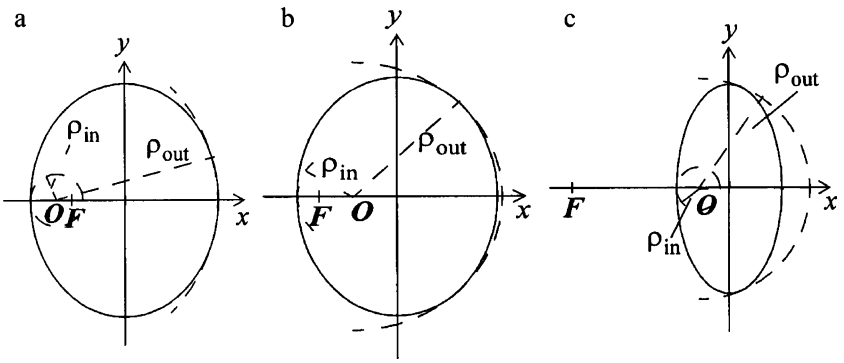

Fig. 5a–c Radii ρ_{in} and ρ_{out} of the material removal profile with ϕ=90° for (**a**) $b>R>(a^2-b^2)/b$, (**b**) $b>(a^2-b^2)/b>R$ and (**c**) $a > \sqrt{2}ba$

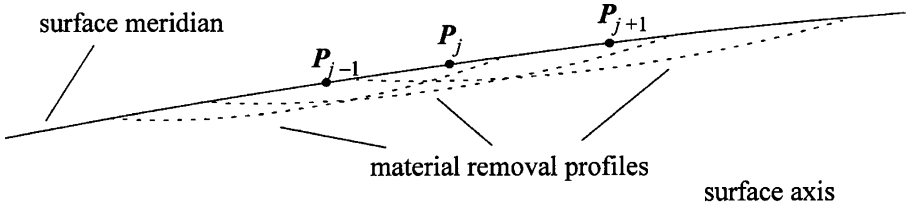

Fig. 6 Paths and the removal profiles along a meridian of an aspheric surface

Point O lies inside the ellipse when $R<a$, as illustrated in Fig. 3b,c. Based on the previous section, ρ_{in} and ρ_{out} of Fig. 1b are given by:

$$\rho_{in} = \begin{cases} a - R & \text{when } a > R > \frac{a^2-b^2}{a} \text{ (Fig.3}b\text{)} \\ b\sqrt{1-\frac{R^2}{a^2-b^2}} & \text{when } a > \frac{a^2-b^2}{a} > R \text{ (Fig. 3}c\text{)} \end{cases} \tag{21}$$

and:

$$\rho_{out} = R + a \tag{22}$$

For $0<\rho\leq\rho_{in}$, the integral in the equation is given by:

$$2\int_0^{\pi} f(\theta)\,\mathrm{d}\,\theta \tag{23}$$

For $\rho_{in}<\rho\leq\rho_{out}$, there may be either one or two solutions of $\cos\theta$ within $(-1, 1)$. The integral is given by the expression in Eq. 20 for the case of one solution. For the case of two solutions, it is given by:

$$2\left[\int_0^{\theta_b^1} f(\theta)\,\mathrm{d}\,\theta + \int_{\theta_b^2}^{\pi} f(\theta)\,\mathrm{d}\,\theta\right] \tag{24}$$

where ${\theta_b}^1$ and ${\theta_b}^2$ correspond to those solutions with $0 < \theta_b^1 < \theta_b^2 < \pi$.

3.3. Major axis of the contact ellipse along the parallels

The major axis of the contact ellipse is along the y direction when ϕ=90° and $(m, n, l)=(a^2, b^2, 0)$ for Eq. 2. Equation 4 becomes:

$$f(\theta) = \sqrt{a^2b^2 - a^2(\rho\cos\theta - \mathrm{R})^2 - b^2\rho^2\sin\theta^2} \tag{25}$$

When $R>b$, point O lies outside the ellipse, as shown in Fig. 4. Based on the results of the last section:

$$\rho_{min} = R - b \tag{26}$$

If $a < \sqrt{2}b$:

$$\rho_{max} = R + b \quad \text{(Fig. 4}a\text{)} \tag{27}$$

If $a > \sqrt{2}b$:

$$\rho_{max} = \begin{cases} R + b & \text{when } R > \frac{a^2-b^2}{a} > b \text{ (Fig. 4}b\text{)} \\ a\sqrt{1+\frac{R^2}{a^2-b^2}} & \text{when } \frac{a^2-b^2}{a} > R > b \text{ (Fig. 4}c\text{)} \end{cases} \tag{28}$$

Equation 1 can be written as:

$$\begin{aligned} &\left(a^2 - b^2\right)\rho^2(\cos\theta)^2 - 2a^2\rho R\cos\theta \\ &\quad -\left(a^2b^2 - a^2R^2 - b^2\rho^2\right) = 0 \end{aligned} \tag{29}$$

For $\rho_{min}<\rho<\rho_{max}$, there can be either one or two solutions of $\cos\theta$ within $(-1, 1)$. For the case of one solution, the integral can be represented by the expression in Eq. 20. For the case of two solutions, it is represented by:

$$2\int_{\theta_b^1}^{\theta_b^2} f(\theta)\,\mathrm{d}\,\theta \tag{30}$$

where ${\theta_b}^1$ and ${\theta_b}^2$ correspond to those solutions and $0 < \theta_b^1 < \theta_b^2 < \pi$.

When $R<b$, point O is within the ellipse, as shown in Fig. 5. In this case, $\rho_{in}=b-R$. If $a < \sqrt{2}b$, $\rho_{out} = b + R$ when $b>R>(a^2-b^2)/b$ (Fig. 5a) and $\rho_{out} = a\sqrt{1+\frac{R^2}{a^2-b^2}}$ when $b>(a^2-b^2)/b>R$ (Fig. 5b). If $a > \sqrt{2}b$ (Fig. 5c), one simply has $\rho_{out} = a\sqrt{1+\frac{R^2}{a^2-b^2}}$.

For $\rho\leq\rho_{in}$, the integral in Eq. 3 is given by the expression in Eq. 23. The evaluation of the integral for $\rho_{in}<\rho\leq\rho_{out}$ is similar to that for $\rho_{min}<\rho<\rho_{max}$. Specifically, the integral is given by Eqs. 20 and 30, respectively.

4. Finishing of aspheric surfaces

The material removal profile computation of the last section is applicable to the planning of aspheric surface finishing. The strategy is to remove a given thickness of material from the surface through abrasives. Circular paths perpendicular to the axis of the aspheric surface would be the natural choice of tool paths. For these paths, the axis of the tool is co-planar with the axis of the surface.

Material removal is affected by the normal force F_n, the spindle speed V, the tool feed rate along the path V_{f0} and the distance between adjacent tool paths. In the present consideration, V is assumed to be constant and F_n is set according to Hertzian contact so that the maximum pressure within the tool–surface contact is constant. When F_n is fixed, the width of the material profile is known for a path point. Thus, the distance between adjacent tool paths is

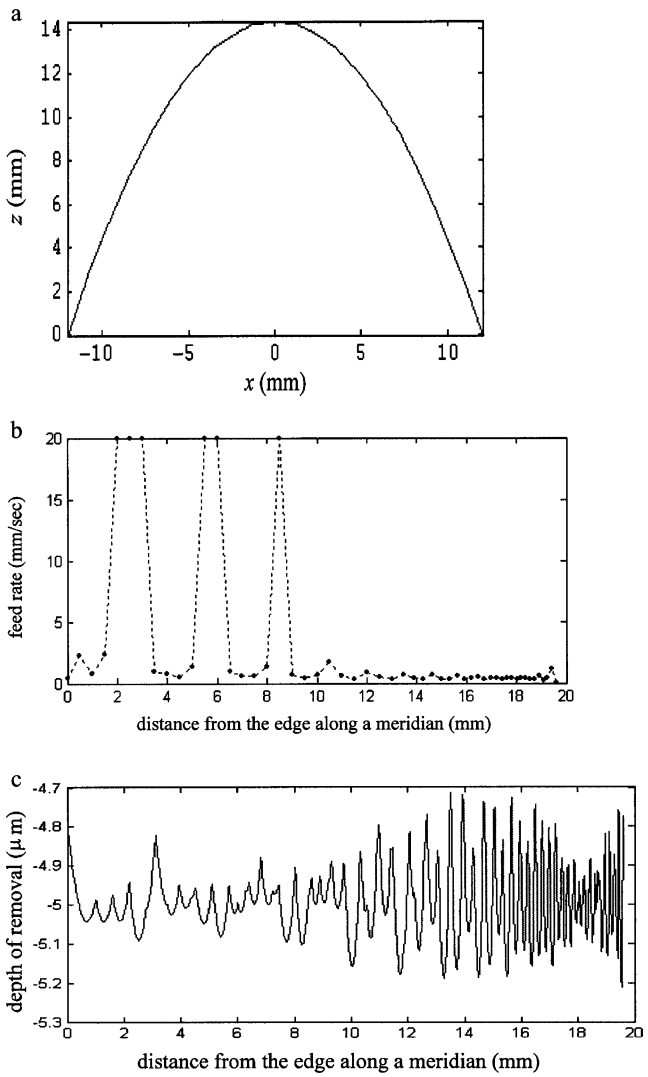

Fig. 7a–c Polishing of a convex paraboloid surface: (**a**) surface cross-section; (**b**) path locations and feed rate; (**c**) material removal

assumed to be a pre-set faction of the material removal profile. In this way, the tool path locations can be fixed.

Let P_j for j=1,..., n be points of the tool paths which line up on the same meridian of the aspheric surface (Fig. 6) and the material removal profile associated with the tool path point P_j. Suppose $d=[d_1,..., d_m]^T$ represent the desired amount of material removal along m equally spaced points along the meridian (m may be a large number so that the distance between adjacent points is very small; for uniform material removal, all elements of d assume the same value). Surface finishing planning may be formulated as:

$$\min_x e^T e \tag{31}$$

where:

$$e = Hx - d \tag{32}$$

represents the error of material removal at the m points, $x=[x_1,..., x_n]^T$ such that $1/x_j$ is the desired feed rate along the

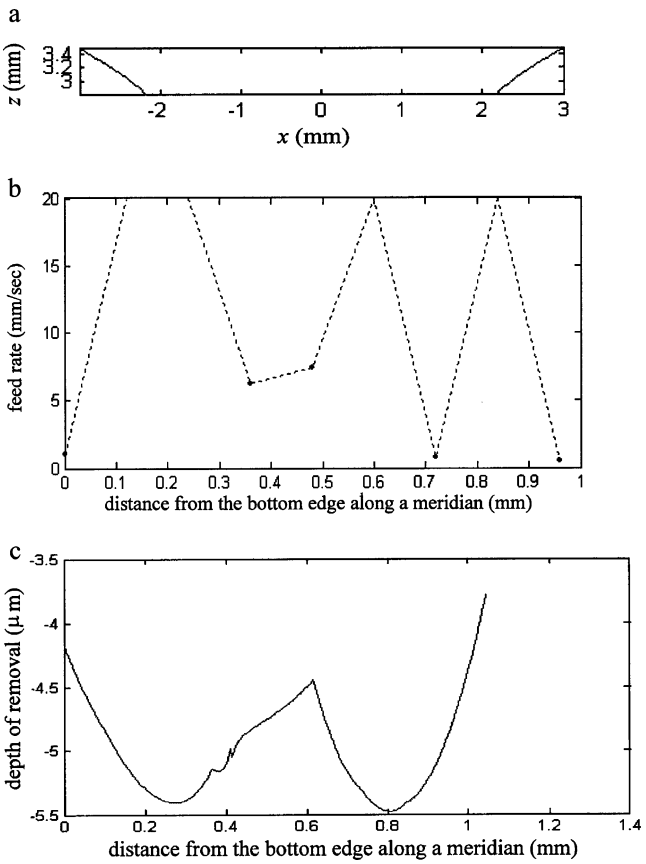

Fig. 8a–c Polishing of a ring inner surface: (**a**) surface cross-section; (**b**) path locations and feed rate; (**c**) material removal

tool path going through point P_j and $H=[h_{ij}]$ is the $m\times n$ matrix such that $[h_{1j},..., h_{mj}]^T$ represents the removal profile at the m points due to the tool path at P_j assuming unity feed rate. The solution to this quadratic optimisation problem is simply the solution of:

$$(H^T H)x = H^T d \tag{33}$$

subject to the constraint $x\geq c>0$ (i.e. so that the permissible feed rates do not exceed $1/c$ for practical reasons), which can be easily obtained from an optimisation problem solver.

5. Examples

Three aspheric steel surfaces are presented to illustrate the proposed surface finishing computation. The surfaces are expressed in parametric form $0\leq u, w\leq 1$. All units of the surfaces are in mm. The material properties of the tool and those of the surfaces are the same as those in [11]. During processing, the tool axis is set perpendicular to the tool path. The spindle speed is adjusted according to the tool size so that the linear speed of the tool relative to the is surface V=942 mm/s.

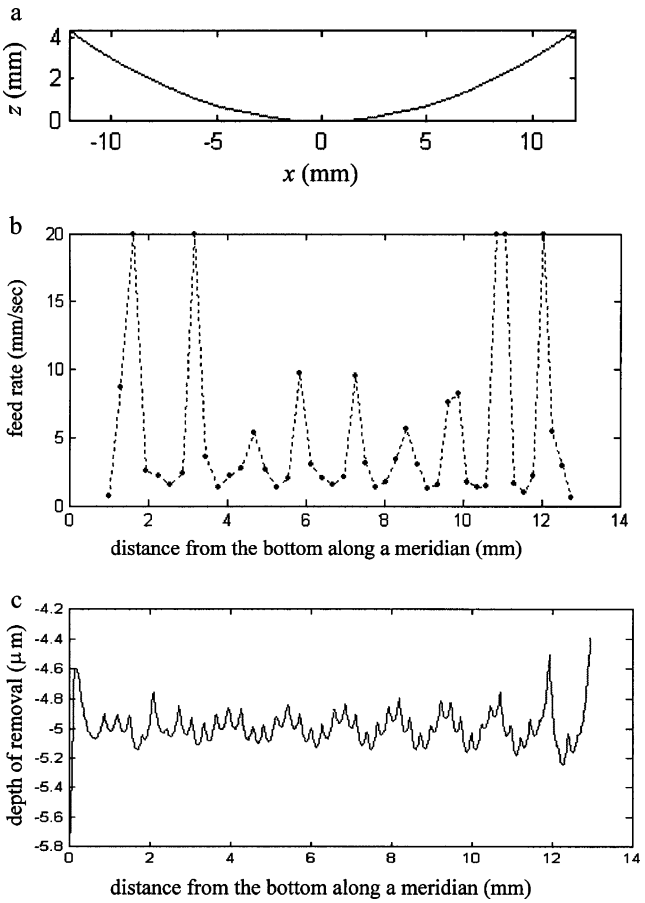

Fig. 9a–c Polishing of a concave paraboloid surface: (**a**) surface cross-section; (**b**) path locations and feed rate; (**c**) material removal

For these surface finishing examples, the target removal depth is 5 μm. The maximum feed rate is set at 20 mm/s. The maximum pressure within the contact ellipse is set at 2 N/mm^2. The distance between adjacent tool paths are selected to be either a pre-set faction of the width of the removal profile or a pre-set value, depending on which is smaller.

The first surface is a convex paraboloid (Fig. 7a):

$$\begin{bmatrix} x \\ y \\ z \end{bmatrix} = \begin{bmatrix} 12w\cos(2\pi u) \\ 12w\sin(2\pi u) \\ 14.4 - 0.1\,(12w)^2 \end{bmatrix} \tag{34}$$

The tool is cylindrical with a 6.5-mm radius. For this example, the major axes of the tool–surface contact ellipse always line up along the meridians of the surface. Calculations of the removal profiles follow Fig. 3a for tool paths away from the top of the surface. The geodesic radius of curvature becomes small and the centre of geodesic curvature falls within the contact ellipse as the tool paths become close to the top of the surface, where the removal profiles follow Fig. 3b. Based on the proposed computation, the location and feed rate of the tool paths for finishing the surface are shown in Fig. 7b and the material removal in Fig. 7c.

The second surface is the inner surface of a ring (Fig. 8a):

$$\begin{bmatrix} x \\ y \\ z \end{bmatrix} = \begin{bmatrix} \left[5 - 4\cos\left(\frac{\pi}{4} + \frac{\pi w}{12}\right)\right]\cos(2\pi u) \\ \left[5 - 4\cos\left(\frac{\pi}{4} + \frac{\pi w}{12}\right)\right]\sin(2\pi u) \\ 4\sin\left(\frac{\pi}{4} + \frac{\pi w}{12}\right) \end{bmatrix} \tag{35}$$

The tool is cylindrical with a 3-mm radius. For this surface, the removal profiles follow Fig. 4; the major axes of the contact ellipse are always along the parallels of the surface. Calculations of $\rho_{\max}$ follows Fig. 4b for tool paths close to the bottom edge, otherwise, $\rho_{\max}$ follows Fig. 4c. The location and feed rate of the tool paths as calculated are shown in Fig. 8b and the resulting material removal in Fig. 8c.

The third surface is a concave paraboloid (Fig. 9a):

$$\begin{bmatrix} x \\ y \\ z \end{bmatrix} = \begin{bmatrix} 15w\cos(2\pi u) \\ 15w\sin(2\pi u) \\ 0.05\,(15w)^2 \end{bmatrix} \tag{36}$$

The tool is spherical with a 7.5-mm radius. The major axes of the contact ellipse are again along the parallels of the surface. The geodesic radius of curvature is small for tool paths close to the bottom of the surface, where calculations of ρ_{in} and ρ_{out} follow Fig. 5a. Otherwise, calculations of the profile follow Fig. 4b. The location and feed rate of the tool paths as calculated are shown in Fig. 9b and the resulting material removal in Fig. 9c.

The simulation results indicate that the depth of removal (Figs. 7c, 8c and 9c) are close to the desired depth of 5 μm. The depth for the first and third surfaces are within +0.2/−0.35 μm and +0.3/−0.6 μm, respectively. The peaks and valleys of the removal curves are consistent with the gaps between adjacent tool paths.

The depth for the second surface varies within +0.5/−1.2 μm, which is less consistent than the other two surfaces but is still acceptable. The main reason is that the length of the meridian is much smaller for this surface—the width of removal profile for some of the tool paths are actually comparable to that length; the number of tool paths that can be fitted on the surface cannot be large.

6. Conclusion

A method for finishing aspheric surfaces using fixed abrasives has been presented in this paper. The strategy is to remove a specified amount of material from the surface during finishing. The method assumes concentric tool paths perpendicular to the axis of the surface. While not imperative, the method also assumes constant spindle speed and the normal force is set such that the maximum pressure

at the tool–surface contact is constant. Efficient computation of the material removal profile for the tool paths is achieved by recognising that the major axis of the contact ellipse is along the direction of either the meridian or the parallel of the surface. The feed rate for the tool paths are obtained through solving a quadratic optimisation problem with linear inequality constraints. The method was applied to compute tool path feed rates for finishing a convex, a concave and a ring surface. The results suggest that the method can facilitate the path planning of abrasive tools. Potential applications of the method are surface finishing processes for the removal of machine marks and the improvement of surface roughness.

Acknowledgement The authors would like to acknowledge the support provided by the Competitive Earmarked Research Grant (CERG, project number CityU 1186/01E) of the Hong Kong Research Grants Council.

References

1. Takeuchi Y, Asakawa N, Ge D-F (1993) Automation of polishing work by an industrial robot (system of polishing robot). JSME Int J C 36(4):556–561
2. Weule H, Timmermann S, Eversheim W (1990) Automation of the surface finishing in the manufacturing of dies and molds. Annals CIRP 39(1):299–303
3. Saito K, Miyoshi T, Sasaki T (1993) Automation of polishing process for a cavity surface on dies and molds by using an expert system. Annals CIRP 42(1):553–556
4. Nowicki B, Szafarczyk M (1993) The new method of free-form surface honing. Annals CIRP 42(1):425–428
5. Stango RJ, Fournelle RA, Chada S (1995) Morphology of surfaces generated by circular wire brushes. J Eng Ind 117:9–15
6. Kunieda M, Nakagawa T, Higuchi T (1988) Robot-polishing of curved surface with magnetically pressed polishing tool. JSPE 54 (1):125–131
7. Mizugaki Y, Sakamoto M, Sata T (1992) Fractal path generation for a metal-mold polishing robot system and its evaluation by the operability. Annals CIRP 41(1):531–534
8. Cho U, Eom DG, Lee DY, Park JO (1992) A flexible polishing robot system for die and mould. In: Proceedings of the 23rd International Symposium on Industrial Robots, Barcelona, Spain, October 1992, pp 449–456
9. Tam H-Y (1999) Toward the uniform coverage of surfaces by scanning curves. Comput Aided Des 31(9):585–596
10. Zhang L, Tam H-Y, Yuan C-M, Chen Y-P, Zhou Z-D (2002) An investigation of material removal in polishing with fixed abrasives. Proc Inst Mech Eng B—J Eng Manuf 216(1):103–112
11. Zhang L, Tam H-Y, Yuan C-M, Chen Y-P, Zhou Z-D, Zheng L (2002) On the removal of material along a polishing path by fixed abrasives. Proc Inst Mech Eng B—J Eng Manuf 216(9):1217–1225
12. Tam H-Y, Zhang L, Meng H (2004) Material removal by fixed abrasives following curved paths. Proc Inst Mech Eng B—J Eng Manuf 218(7):713–720